Nanostructured Transparent Conductive Electrodes for Applications in Harsh Environments Fabricated via Nanosecond Laser-Induced Periodic Surface Structures (LIPSS) in Indium–Tin Oxide Films on Glass

Hendrik Martin Reinhardt, Philipp Maier, Hee-Cheol Kim, Daniel Rhinow, and Norbert Hampp*

A self-organization phenomenon named laser-induced periodic surface structures (LIPSS) is utilized for pattern formation in indium–tin oxide (ITO) transparent conductive films coated on borosilicate glass. Stripe patterns with periodicities down to 175 nm are created by scanning the focused beam (30 µm spot diameter 1 e^{-2}) of a nanosecond pulsed laser operating at 532 nm wavelength over ITO films. Highly ordered ITO-LIPSS are generated at a pulse duration of 6 ns, pulse frequencies between 100 and 200 kHz, pulse energies around 20 µJ, and laser spot scan speeds in the range of 50–80 mm s^{-1}. Resulting nanopatterns are electrically conductive and feature improved optical transparency as well as stability against strong acids such as hydrochloric acid, sulfuric acid, and even aqua regia. The formation of mixed phases between ITO and silicon is considered to be the origin for the chemical robustness of laser patterned transparent conductive electrodes.

1. Introduction

Indium–tin oxide (ITO) is widely applied for the manufacture of light-emitting devices, touch panels, solar cells, sensors, smart glass, and more.[1–7] High optical transmittance combined with remarkable electrical conductivity makes ITO the most commonly used transparent conductor. The fabrication of high-quality ITO films is typically performed via magnetron sputtering on glass or substrates such as polyethylene terephthalate and polycarbonate.[8,9] Alternative coating techniques include ion-beam-assisted deposition and pulsed laser deposition as well as dip coating and metalorganic chemical vapor deposition.[10–13] Mentioned techniques yield continuous ITO films which are patterned in a further processing step. As lithographic processes for ITO patterning are time consuming and pollutive, alternative methods gain increasing interest.

Laser-based patterning performs well in this domain since lasers facilitate contactless, fast, and reliable micromachining over extended surface areas. On the production scale, direct laser ablation of ITO thin films achieves spatial resolutions in the range of 5–50 µm.[14–16] Feature sizes down to the submicron scale can be realized on the laboratory scale; however, industrial use of laser direct writing with submicron resolution is barely viable due to prohibitively long processing times required for pattern formation over extended surface areas.[17–19] An elegant solution for submicron patterning with high throughput is the utilization of laser-stimulated self-organization. In particular, a phenomenon called laser-induced periodic surface structures (LIPSS) offers great potential for robust submicron patterning over extended surface areas.[20–22] The formation of LIPSS in ITO has already been demonstrated. Studies concerning this topic were conducted with ultrafast lasers and are primarily focused on alterations of structural and chemical aspects or rather changes of the electrical and optical properties of ITO resulting from LIPSS generation.[23–29] In general, LIPSS are stimulated when a material is subjected to pulsed laser irradiation under conditions that trigger specific light-matter feedback mechanisms. Performed with nanosecond pulsed lasers, this characteristically generates surface ripples featuring periodicities close to the laser wavelength which are currently referred to as low-spatial frequency LIPSS (LSFL).[30] The exact mechanism of LIPSS formation is still under debate. LSFL are currently regarded as the result of interference between incident wave fronts and surface scattered waves or rather surface plasmon polaritons.[31–35] Resulting fringe patterns transpose their periodically alternating photonic flux densities into morphological, structural, and compositional transformations that can give rise to electrical, catalytic, and magnetic surface patterns.[36] In this study, LIPSS are utilized for the rapid patterning of ITO films coated on borosilicate glass. The process is performed by scanning the focused beam of a linearly polarized nanosecond pulsed laser over the substrate. Resultant LIPSS are oriented parallel with regard to laser polarization and feature an average periodicity of 350 nm at normal laser beam incidence.

Dr. H. M. Reinhardt, P. Maier, Dr. H.-C. Kim, Dr. D. Rhinow, Prof. N. A. Hampp
Philipps-University of Marburg
Department of Chemistry
Hans-Meerwein-Str. 4, 35032 Marburg, Germany
E-mail: Hendrik.Reinhardt@staff.uni-marburg.de

Investigations on the morphological, structural, and chemical effects of LIPSS formation in the system ITO/glass indicate the diffusion of silica into ITO, thus creating a mixed phase. Besides electrical conductivity, distinguishing features of this phase are robustness against strong acids as well as high optical transmittance. Moreover, the mixed phase features a pattern periodicity of 175 nm which is quite unusual for LIPSS generated by a nanosecond pulsed laser operating at a wavelength of 532 nm.

2. Results and Discussion

Submicron-patterning of ITO is demonstrated by means of LIPSS formation in ITO films of 170 nm thickness coated on borosilicate glass. The smiley illustrated in **Figure 1**a was created by scanning a laser spot of 30 µm diameter with a line scan speed of 80 mm s^{-1} and a line spacing of 10 µm across the sample surface. An easy way to verify the successful generation of periodic patterns or rather LIPSS is the typical white light diffraction when lit by a lamp. The detailed inspection of LIPSS in the system ITO/glass by scanning electron microscopy (SEM) shows a regular stripe pattern with an average periodicity of 350 nm (Figure 1b). LIPSS can also be generated in the form of single line scans (Figure 1c), as the white light diffraction of Fibonacci spirals in Figure 1d demonstrates.

Irrespective of the scanned geometry, LIPSS in the system ITO/glass always feature parallel orientation with respect to the laser polarization. A result like this is typically observed in the case of LSFL (low-spatial frequency LIPSS) generated on dielectrics using a linearly polarized nanosecond laser. In the particular case, this outcome could be explained by LIPSS formation at the interface of the dielectric glass substrate. Alternatively, it could be argued that the orientation of LIPSS is not affected by the electric properties of ITO but rather by its optical properties which resemble a dielectric. In order to find out at which of the two interfaces LIPSS were actually generated, experiments under different angles of laser irradiation were conducted. The angle of laser beam incidence has an impact on the periodicity of generated LIPSS, as illustrated in **Figure 2**a. In general, the LIPSS periodicity increases with increasing angle of laser beam incidence. Yet there are differences in the extent to which LIPSS periodicities are affected by angular laser irradiation. In the case of s-polarized light, the periodicity of LIPSS almost doubles (700 nm) when the angle of laser beam incidence is set to 50°. By contrast, a p-polarized laser beam generates LIPSS with periodicities of ≈400 nm at the same angle of incidence. For both polarizations, good correlations between experimentally observed and theoretically derived periodicities are found when the refractive index of the borosilicate glass substrate ($n = 1.514$) is used for calculations based on the model of Bäuerle and Bonch-Bruevich (Figure 2b).[37,38] As this is not the case for calculations based on the refractive index of ITO ($n = 1.826$), the formation of LIPSS is considered to take place at the interface to the glass substrate. In order to obtain insights into the mechanisms of LIPSS formation, the morphology, the composition, and the structure of LIPSS in the system ITO/glass were examined. **Figure 3**a shows a cross-sectional view of the system under investigation before and after laser modification. Backscattered electron imaging enables a clear distinction between the glass substrate and the ITO thin film on its surface. Prior to the laser modification, ITO features a film thickness of 170 nm. LIPSS formation causes ablation yielding a periodic wave structure with an average periodicity of 350 nm and an average thicknesses of 70 nm at peak positions and 40 nm at valley positions. The wave pattern is considered to be caused by an optical stimulus with a spatially varying intensity profile. A recent study confirmed the transient occurrence of so-called photonic fringe patterns during LIPSS formation.[39] Compositional mappings of ITO-LIPSS conducted with energy-dispersive X-ray spectroscopy (EDX) show periodically varying concentrations of indium, tin, and silicon (Figure 3b). Peaks in the elemental distributions of indium and tin are located at topographic maxima, whereas peaks of silicon are located in topographic minima. This result is interpreted as a representation of the thickness modulations in ITO films after LIPSS formation. Structural analyses via X-ray powder diffraction (XPD) indicate ITO-LIPSS to comprise crystalline sites, although to a much lesser extent compared to ITO thin films annealed in a furnace at 200 °C or rather 500 °C (Figure 3c). Nevertheless, the formation of LIPSS is accompanied by crystallization as the comparison of XPD spectra obtained from as-deposited ITO and ITO-LIPSS shows. Etching studies were conducted in order to investigate the spatial distribution of crystalline ITO in ITO-LIPSS. The approach exploits the fact that the etch rate in
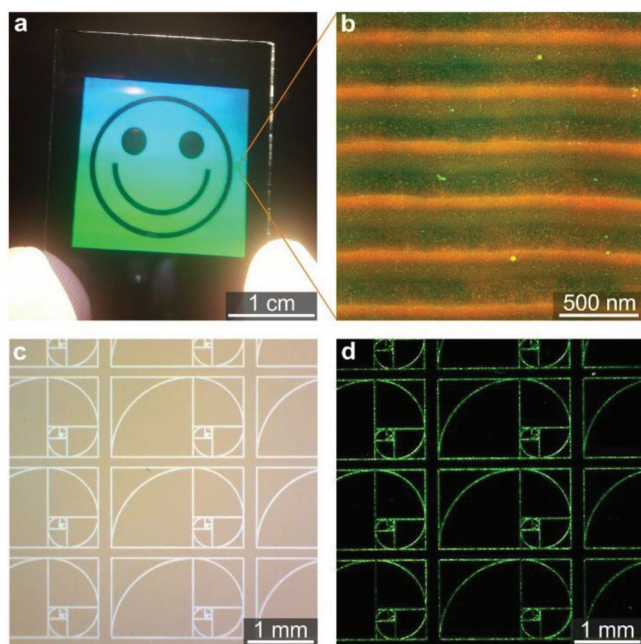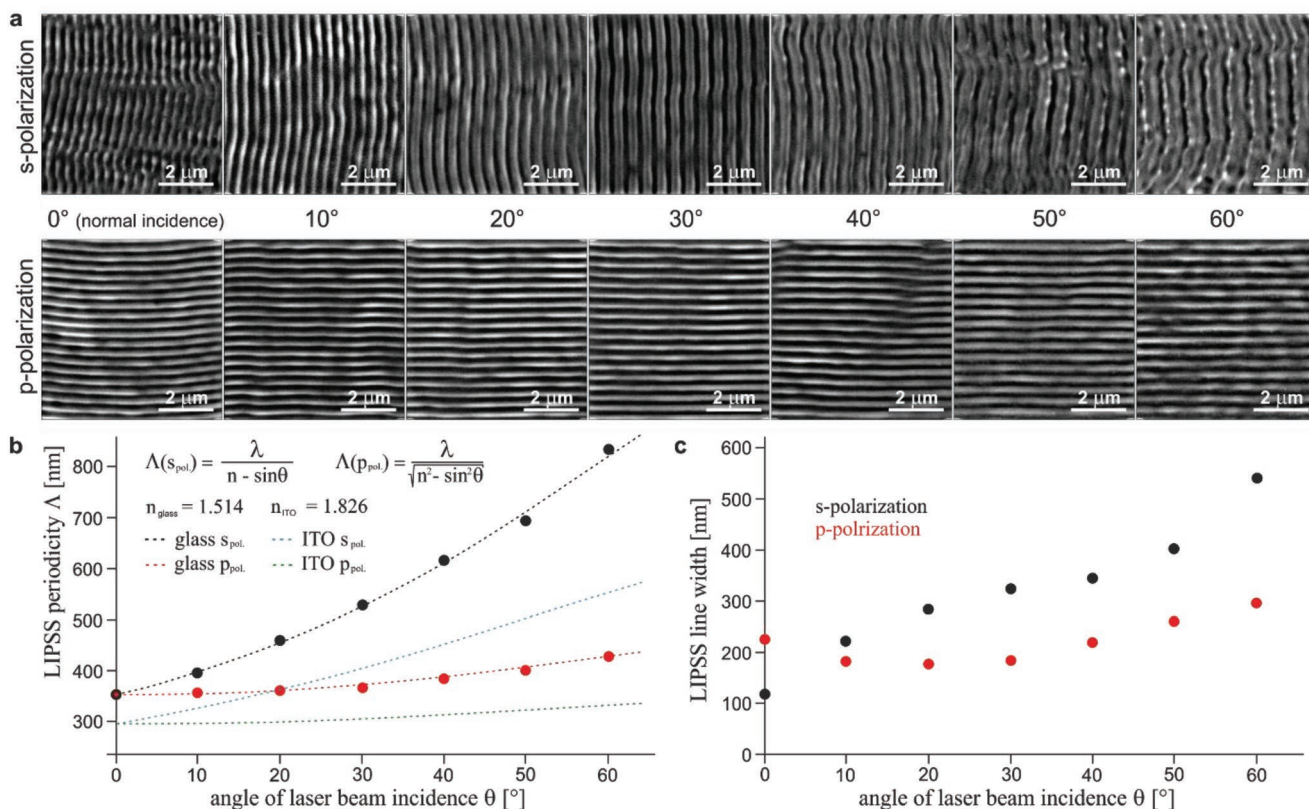

Figure 1. Generation of ITO-LIPSS. a) Photo of white light diffraction from a smiley pattern generated on an ITO-coated glass slide using the following irradiation parameters: pulse energy 20 µJ, peak fluence 5.6 J cm^{-2}, pulse frequency 200 kHz, line scan speed 80 mm s^{-1}, line spacing 10 µm, 59 pulses per spot diameter. b) Electron micrograph of LIPSS in the system ITO/glass with superposition of morphological contrast (green, secondary electron imaging) and material contrast (orange, backscattered electron imaging). c) Array of Fibonacci spirals on ITO-coated glass. Irradiation parameters: pulse energy 20 µJ, peak fluence 5.6 J cm^{-2}, pulse frequency 100 kHz, line scan speed 50 mm s^{-1}, 47 pulses per spot diameter. d) Photo of white light diffraction from Fibonacci spirals demonstrating the existence of LIPSS in laser-written single lines.

Figure 2. Relation of LIPSS periodicity and the angle of laser beam incidence. a) SEM images of LIPSS generated on ITO/glass at laser beam's angle of incidence from 0–60° for s-polarization (top row) and p-polarization (lower row). Irradiation parameters: pulse energy 20 μJ, peak fluence 5.6 J cm^{-2}, pulse frequency 120 kHz, line scan speed 55 mm s^{-1}, line spacing 10 μm, 51 pulses per spot diameter. b) Plot of experimentally observed LIPSS periodicities versus angles of laser beam incidence for s-polarization (black dots) and p-polarization (red dots). Dotted lines show the correlation between experimentally observed and theoretical LIPSS periodicity and the laser beam's angle of incidence derived by the model of Bäuerle and Bonch-Bruevich.[37,38] Calculations are based on depicted equations using a laser wavelength of 532 nm and a refractive index of $n = 1.514$ which resembles the borosilicate glass substrate and $n = 1.826$ which resembles the ITO coating. c) Plot of ITO-LIPSS line widths versus the angles of laser beam incidence for s-polarization (black dots) and p-polarization (red dots).

mineral acids is one order of magnitude higher for amorphous ITO compared to crystalline ITO.[40] Etching in hydrochloric acid was found to inflict distinct morphological changes of ITO-LIPSS, as AFM topographies recorded prior (**Figure 4**a) and after (Figure 4b) the acid treatment demonstrate. While untreated ITO-LIPSS feature a washboard-like morphology with amplitudes in the range of 40 nm, the peak heights of etched ITO-LIPSS are significantly reduced. Moreover, a morphological transformation from single to double peaks featuring peak-to-peak distances of about 160 nm is observed (Figure 4c). These results lead to the conclusion that peak regions of ITO-LIPSS predominantly comprise amorphous ITO which is readily dissolved by hydrochloric acid whereas the peripheral zones of the periodic ribbons are less affected by acid, thus indicating to comprise larger fractions of crystalline ITO. The transformation of ITO-LIPSS into a pattern with an average periodicity of 175 nm is intriguing since LIPSS of this scale are normally only accessible with ultraviolet or rather femtosecond lasers (HSFL).[41–43] Acid treatment also has a positive impact on the optical properties of ITO-LIPSS, as transmission spectra show (Figure 4d). In fact, the transmittance of acid-treated ITO-LIPSS is almost as high as the transmittance of the uncoated borosilicate glass. Even after prolonged immersion in

strong acids electrical conductivity is still provided, as electrochemical depositions of polyaniline (Figure 4e) and silver (Figure 4f) on ITO-LIPSS demonstrate. Polyaniline (PANI) was deposited by cyclic voltammetry from an electrolyte containing 2 mol L^{-1} sulfuric acid and 0.2 mol L^{-1} aniline. The electrochemical polymerization to PANI took place with spatial selectivity matching the pattern of ITO-LIPSS (Figure 4e). This result demonstrates the stability of the patterned electrode against an oxidizing acid for an exposure time of several minutes. Not even immersion in aqua regia (HCl/HNO$_3$ 3:1) for a duration of 8 h eliminated the electrical conductance of ITO-LIPSS but solely impaired its optical properties. (Figure 4d). The electrochemical reduction of silver ions on ITO-LIPSS pretreated in aqua regia for a period of 8 h leads to spatially selective depositions of silver nanoparticles preferably along the edges of the 160 nm double-peak pattern. The astonishing resistance of ITO-LIPSS against acid is proposed to originate from silicon incorporations into ITO upon LIPSS formation. The possibility of mixed phase formation between silicon and ITO is described in a study of Ow-Yang, who investigated interfacial reactions emergent during sputter deposition of ITO onto silicon. The group postulated the formation of ternary phases.[44] Their results have been confirmed by research
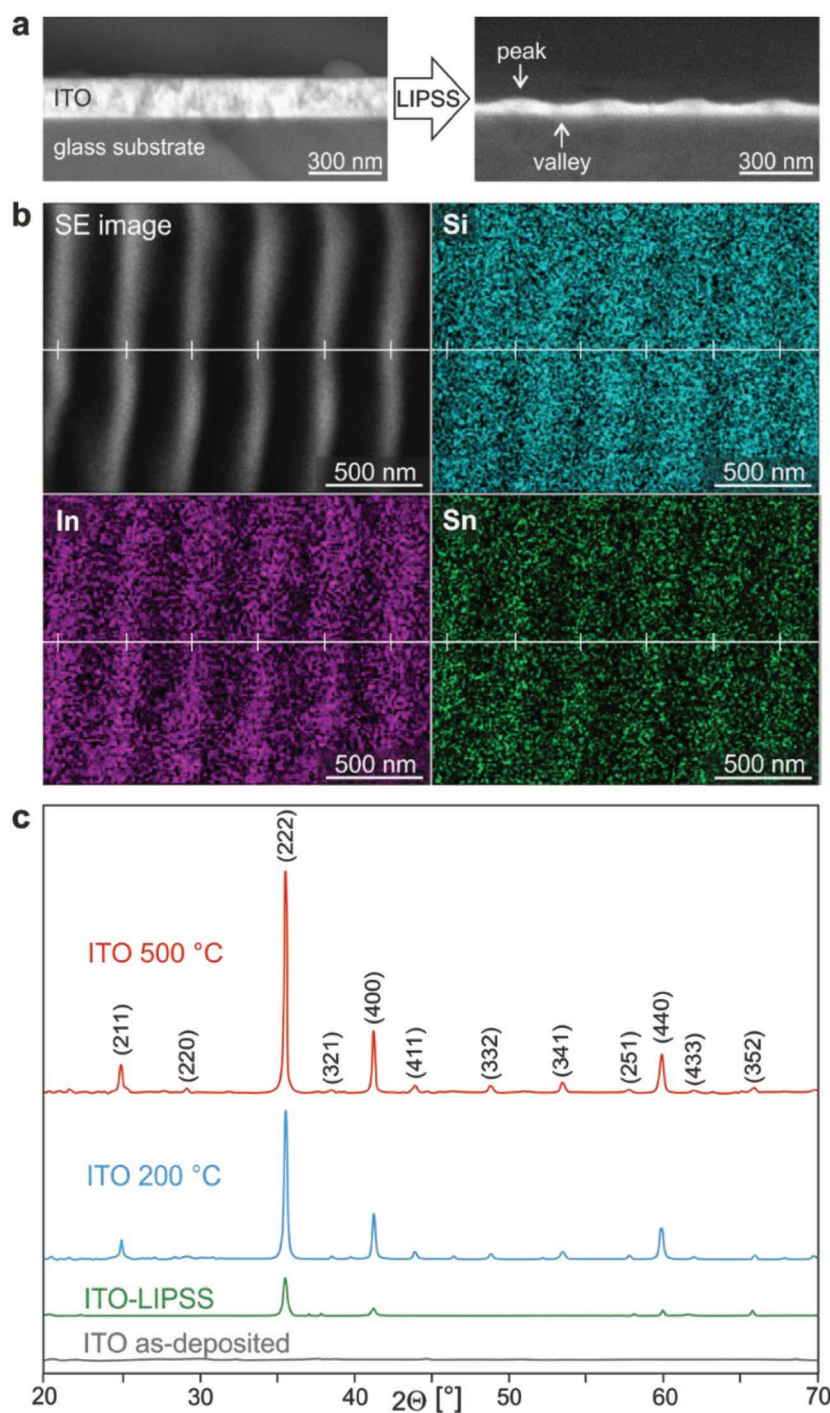
Figure 3. Morphology, composition, and structure of LIPSS in the system ITO/glass. a) Cross-sectional SEM view on ITO thin film on glass before (left) and after LIPSS formation (right). b) Energy dispersive X-ray spectroscopy (EDX) mapping of LIPSS-modified ITO/glass including secondary electron image (SE) as well as X-ray lines Si Kα1, In Lα1, and Sn Lα1. c) X-ray powder diffraction (XPD) of 170 nm ITO film on borosilicate glass (as-deposited), LIPSS-modified ITO/glass (ITO-LIPSS) and ITO thin films on borosilicate glass heat treated at 200 °C and 500 °C in a furnace under ambient atmosphere. All investigations were performed on ITO-LIPSS generated with the following irradiation parameters: pulse energy 20 µJ, peak fluence 5.6 J cm^{-2}, pulse frequency 120 kHz, line scan speed 55 mm s^{-1}, line spacing 10 µm, 51 pulses per spot diameter.

groups around Kim and Ma.[45,46] In particular, advanced XPS studies conducted by Ma point toward ternary phases forming at the interface between ITO and SiO$_x$ at a temperature of

250 °C.[47] During LIPSS formation, photo-thermal heating causes surface temperatures by far exceeding 250 °C. It is therefore reasonable to assume that thermally enhanced kinetics at the interface between ITO and borosilicate glass lead to the formation of mixed phases. To our knowledge, there are no records concerning the advanced stability of such phases in harsh environments. The chemical stability of transparent conductive electrodes is becoming increasingly important for the practical applicability of upcoming technologies. This is particularly the case in application fields such as sensors, light emitters, and organic solar cells where nanostructured transparent conducting electrodes are a distinguishing factor of device performance.[48–52]

3. Conclusion

The formation of ITO-LIPSS over extended surface areas is demonstrated by scanning a linearly polarized nanosecond pulsed laser beam with a wavelength of 532 nm over ITO-coated borosilicate glass. ITO-LIPSS are oriented in parallel direction with respect to the laser polarization. The relation between the angle of laser beam incidence and the resulting ripple periodicity indicates LIPSS to be formed at the interface between ITO and the glass substrate. Besides morphological changes, LIPSS formation on ITO-coated borosilicate glass induces structural and chemical transformations. Acid treatment turns ITO-LIPSS with an initial pattern periodicity of 350 nm into a pattern featuring an average periodicity of 175 nm. This sub-pattern results from selective etching of ITO in the central zones of the periodic ribbons whereas the edge zones of these ribbons persist. Electrical conductivity is still present after acid treatment as selective electrodepositions of polyaniline and silver nanoparticles on the 175 nm subpattern demonstrate. The incorporation of silicon into indium–tin oxide is considered to be the reason for the robustness of this subpattern against acidic environments.

4. Experimental Section

Borosilicate glass slides (100 × 100 × 0.63 mm^3) coated with indium–tin oxide (ITO) in a film thickness of 170 nm were supplied by Dr. Feodor Oestreicher (fluessigkristalle.com, Berlin, Germany). The refractive indices of borosilicate glass ($n = 1.514$) and of the ITO coating ($n = 1.826$) at a wavelength of 532 nm were determined using a multiwavelength-refractometer DSR-λ (Schmidt & Haensch, Germany).
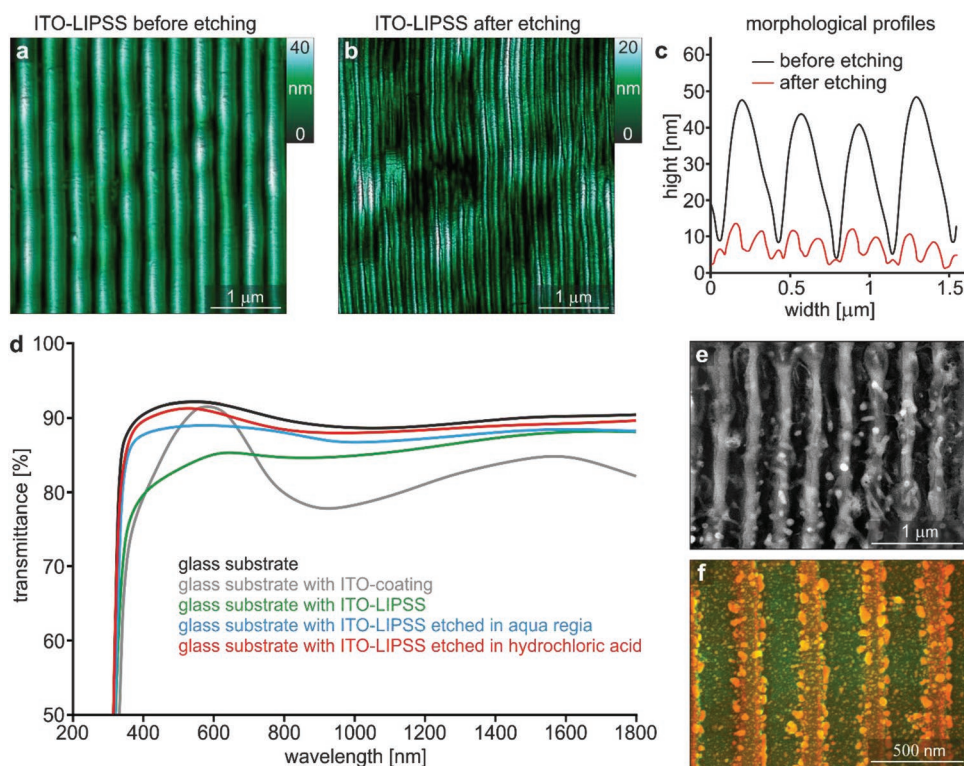
Figure 4. Acid stability of ITO-LIPSS transparent conductive electrodes. AFM scan of ITO-LIPSS before a) and after acid treatment b) in 6 M HCl. c) Morphological profiles before and after acid treatment in 6 M HCl. d) Comparative transmittance spectra of base substrates (borosilicate glass, with and without 170 nm ITO film) and laser-modified substrates (ITO-LIPSS) before and after acid treatment. e) SEM image of polyaniline (PANI) electrodeposited on ITO-LIPSS pretreated in 6 M HCl. f) SEM image of silver nanoparticles deposited on ITO-LIPSS pretreated with aqua regia for 8 h. The colors result from superposition of morphological contrast (green, secondary electron imaging) and material contrast (orange, backscattered electron imaging). All investigations were performed on ITO-LIPSS generated with the following irradiation parameters: pulse energy 20 µJ, peak fluence 5.6 J cm^{-2}, pulse frequency 120 kHz, line scan speed 55 mm s^{-1}, line spacing 10 µm, 51 pulses per spot diameter.

The formation of LIPSS in the system ITO/glass was performed using a linearly polarized nanosecond pulsed laser (Explorer XP-532, Newport, USA) emitting laser pulses of 6 ns pulse width at a wavelength of 532 nm. The laser beam (beam profile TEM$_{00}$, $M^2 < 1.1$) was focused to a spot size of 30 µm diameter (1 e^{-2}) using an F-theta lens (f-163-532, Rodenstock, Germany) and scanned over substrates using a galvanometer scan head (SCANgine 14-532, Scanlab, Germany). The formation of LIPSS on ITO-coated borosilicate glass requires a minimum pulse energy of 13 µJ or rather a min. laser fluence of 1.84 J cm^{-2}. High-quality ITO LIPSS were generated with pulse energies around 20 µJ, pulse frequencies between 100 and 200 kHz, and laser spot scan speeds in the range of 50–80 mm s^{-1}. Specific irradiation parameters for the generation of ITO-LIPSS used as examples in this study are provided in the respective figure captions.

The electrochemical deposition of polyaniline (PANI) onto ITO-LIPSS was performed with a potentiostat/galvanostat (Model 273A, EG&G Princeton Applied Research, USA). ITO-LIPSS were contacted as the working electrode in an electrolyte containing 2 M H$_2$SO$_4$ and 0.2 M aniline in distilled water. The PANI coating on ITO-LIPSS was obtained by cyclic voltammetry between the potentials of 0.2 and 0.8 V (30 cycles at 100 mVs^{-1}). Silver nanoparticles were deposited on ITO-LIPSS contacted as the working electrode in an aqueous electrolyte containing 0.05 M AgNO$_3$ and 0.1 M KNO$_3$ at a potential of −1.4 V for a duration of 100 s.

Scanning electron microscopy (SEM) was performed on a field emission microscope (JSM-7500F, Jeol, Japan) equipped with a backscattered electron detector (BSE, Autrata, Czech Republic). Operated at 10 kV, the maximum spot resolution of the JSM-7500F was 1.2 nm.

Energy-dispersive X-ray spectroscopy (EDX) was performed on an Auriga (Zeiss, Germany) scanning electron microscope equipped with an 80 mm^2 detector (AZtec, Oxford Instruments, England).

Crystal structure analyses were performed on an X'Pert PRO MPD (PANalytical, Netherlands) powder diffractometer equipped with X'Pert tube Co LFF operating at 40 kV and 30 mA. Diffractograms were recorded in the range of $20° \leq 2\theta \leq 70°$ and an angular resolution of $0.1° 2\theta$ at room temperature. X'Pert High Score Plus v2.2c was used for data processing and analysis.

Transmittance spectra were recorded on a Lambda 1050 UV/VIS/NIR spectrometer (PerkinElmer, USA) equipped with 3D WB detector module in a wavelength range of 200–1800 nm and a resolution of 1 nm.

Surface topographies of ITO-LIPSS were recorded using an atomic force microscope (Nanoscope 8, Bruker, USA). Scans were performed in tapping mode with SCM-PIT tips (antimony-n-doped Si, spring constant 1–5 N m^{-1}, frequency 60–100 kHz). The scan angle was 45° with respect to the orientation of ITO-LIPSS.

Conflict of Interest

The authors declare no conflict of interest.

Keywords

[1] D. Ginley, H. Hosono, D. C. Paine, *Handbook of Transparent Conductors*, Springer, Germany **2010**.

[2] M. K. Choi, J. Yang, D. C. Kim, Z. Dai, J. Kim, H. Seung, V. S. Kale, S. J. Sung, C. R. Park, N. Lu, T. Hyeon, D.-H. Kim, *Adv. Mater.* **2018**, *30*, 1703279.

[3] N. M. Sangeetha, M. Gauvin, N. Decorde, F. Delpech, P. F. Fazzini, B. Viallet, G. Viau, J. Grisolia, L. Ressier, *Nanoscale* **2015**, *7*, 12631.

[4] D. van Dam, N. J. J. van Hoof, Y. Cui, P. J. van Veldhoven, E. P. A. M. Bakkers, J. G. Rivas, J. E. M. Haverkort, *ACS Nano* **2016**, *10*, 11414.

[5] W. Wang, H. Peng, S. Chen, *J. Mater. Chem. C* **2016**, *4*, 1838.

[6] B. C. Yadav, K. Agrahari, S. Singh, T. P. Yadav, *J. Mater. Sci.: Mater. Electron.* **2016**, *27*, 4172.

[7] M. Laurenti, S. Bianco, M. Castellino, N. Garino, A. Virga, C. F. Pirri, P. Mandracci, *ACS Appl. Mater. Interfaces* **2016**, *8*, 8032.

[8] Z. Ghorannevis, E. Akbarnejad, M. Ghoranneviss, *J. Theor. Appl. Phys.* **2015**, *9*, 285.

[9] J. R. Lee, D. Y. Lee, D. G. Kim, G. W. Lee, Y. D. Kim, P. K. Song, *Met. Mater. Int.* **2008**, *14*, 745.

[10] C. Liu, T. Mihara, T. Matsutani, T. Asanuma, M. Kiuchi, *Solid State Commun.* **2003**, *126*, 509.

[11] K. A. Sierros, D. R. Cairns, J. S. Abell, S. N. Kukureka, *Thin Solid Films* **2010**, *518*, 2623.

[12] O. O. Akinwunmi, M. A. Eleruja, J. O. Olowolafe, G. A. Adegboyega, E. O. B. Ajayi, *Opt. Mater.* **1999**, *13*, 255.

[13] T. Ito, H. Uchiyama, H. Kozuka, *Langmuir* **2017**, *33*, 5314.

[14] O. Yavas, M. Takai, *Appl. Phys. Lett.* **1998**, *73*, 2558.

[15] S. Venkat, C. Dunsky, in *Proc. 2006, Lasers and Applications in Science and Engineering*, SPIE, San Jose **2006**, *6106*, 610608.

[16] U. Geyer, J. Hauss, B. Riedel, S. Gleiss, U. Lemmer, M. Gerken, *J. Appl. Phys.* **2008**, *104*, 093111.

[17] R. Sahin, I. Kabacelik, *Appl. Phys. A* **2016**, *122*, 314.

[18] M. Afshar, M. Straub, H. Voellm, D. Feili, K. Koenig, *Opt. Lett.* **2012**, *37*, 563.

[19] C.-W. Cheng, C.-Y. Lin, *Appl. Surf. Sci.* **2014**, *314*, 215.

[20] H. M. Reinhardt, K. Bücker, N. A. Hampp, *Opt. Express* **2015**, *23*, 11965.

[21] I. Gnilitskyi, T. J. Y. Derrien, Y. Levy, N. M. Bulgakova, T. Mocek, L. Orazi, *Sci. Rep.* **2017**, *7*, 8485.

[22] A. Ruiz de la Cruz, R. Lahoz, J. Siegel, G. F. de la Fuente Solis, *Opt. Lett.* **2014**, *39*, 2491.

[23] C. W. Cheng, W. C. Shen, C. Y. Lin, Y. J. Lee, J. S. Chen, *Appl. Phys. A* **2010**, *101*, 243.

[24] C. Wang, H.-I. Wang, W.-T. Tang, C.-W. Luo, T. Kobayashi, J. Leu, *Opt. Express* **2011**, *19*, 24286.

[25] M. Afshar, M. Straub, H. Voellm, D. Feili, K. König, H. Seidel, *Opt. Lett.* **2012**, *37*, 563.

[26] C. Wang, H.-I Wang, C.-W. Luo, J. Leu, *Appl. Phys. Lett.* **2012**, *101*, 101911.

[27] M. Afshara, M. Lebera, W. Poppendieck, K. König, H. Seidel, D. Feili, *Appl. Surf. Sci.* **2016**, *360*, 494.

[28] A. Cerkauskaite, R. Drevinskas, A. Solodar, I. Abdulhalim, P. G. Kazansky, *ACS Photonics* **2017**, *4*, 2944.

[29] P. Liu, W. Wang, A. Pan, Y. Xiang, D. Wang, *Opt. Laser Technol.* **2018**, *106*, 259.

[30] N. R. Isenor, *Appl. Phys. Lett.* **1977**, *31*, 148.

[31] J. E. Sipe, J. F. Young, J. S. Preston, H. M. van Driel, *Phys. Rev. B* **1983**, *27*, 1141.

[32] J. F. Young, J. S. Preston, H. M. van Driel, J. E. Sipe, *Phys. Rev. B* **1983**, *27*, 1155.

[33] P. Nürnberger, H. M. Reinhardt, H.-C. Kim, E. Pfeifer, M. Kroll, S. Müller, F. Yang, N. A. Hampp, *Appl. Surf. Sci.* **2017**, *425*, 682.

[34] J. Bonse, A. Rosenfeld, J. Krüger, *J. Appl. Phys.* **2009**, *106*, 104910.

[35] F. Garrelie, J. P. Colombier, F. Pigeon, S. Tonchev, N. Faure, M. Bounhalli, S. Reynaud, O. Parriaux, *Opt. Express* **2011**, *19*, 9035.

[36] H. Reinhardt, H.-C. Kim, C. Pietzonka, J. Kruempelmann, B. Harbrecht, B. Roling, N. Hampp, *Adv. Mater.* **2013**, *25*, 3313.

[37] D. Bäuerle, *Laser Processing and Chemistry*, Springer, Germany **2011**.

[38] A. M. Bonch-Bruevich, M. N. Libenson, V. S. Makin, V. V. Trubaev, *Opt. Eng.* **1992**, *31*, 718.

[39] H. Reinhardt, P. Peschke, R. Riedel, N. Hampp, *Nanotechnology* **2018**, *29*, 305303.

[40] U. Betz, M. Kharrazi Olsson, J. Marthy, M. F. Escolá, F. Atamny, *Surf. Coat. Technol.* **2006**, *200*, 5751.

[41] D. Dufft, A. Rosenfeld, S. K. Das, R. Grunwald, J. Bonse, *J. Appl. Phys.* **2009**, *105*, 034908.

[42] P. Calvani, A. Bellucci, M. Girolami, S. Orlando, V. Valentini, A. Lettino, D. M. Trucchi, *Appl. Phys. A* **2014**, *117*, 25.

[43] F. Fraggelakis, G. Mincuzzi, I. Manek-Hönninger, J. Lopez, R. Kling, *RSC Adv.* **2018**, *8*, 16082.

[44] C. W. Ow-Yang, Y. Shigesato, D. C. Paine, *J. Appl. Phys.* **2000**, *88*, 3717.

[45] H. Kim, S.-H. Hong, Y. C. Park, J. Lee, C.-H. Jeon, J. Kim, *Mater. Lett.* **2014**, *115*, 45.

[46] H. W. Du, J. Yang, Y. H. Li, F. Xu, J. Xu, Z. Q. Ma, *Appl. Phys. Lett.* **2015**, *106*, 093508.

[47] S. Chen, M. Gao, Y. Wan, H. Du, Y. Li, Z. Ma, *Appl. Surf. Sci.* **2016**, *388*, 57.

[48] D. Lin, K. D. Harris, N. W. C. Chan, A. B. Jemere, *Sens. Actuators, B* **2018**, *257*, 324.

[49] E. González-Arribas, T. Bobrowski, C. D. Bari, K. Sliozberg, R. Ludwig, M. D. Toscano, A. L. De Lacey, M. Pita, W. Schuhmann, S. Shleev, *Biosens. Bioelectron.* **2017**, *97*, 46.

[50] C.-Y. Chen, W.-K. Lee, Y.-J. Chen, C.-Y. Lu, H. Y. Lin, C.-C. Wu, *Adv. Mater.* **2015**, *27*, 4883.

[51] K. R. Son, T. H. Lee, B. R. Lee, H. S. Im, T. G. Kim, *Small* **2018**, *14*, 1870234.

[52] B. Cao, X. He, J. B. Sorge, A. Lalany, K. Ahadi, A. Afshar, B. C. Olsen, T. C. Hauger, M. H. Mobarok, P. Li, K. C. Cadien, M. J. Brett, E. J. Luber, J. M. Buriak, *ACS Appl. Mater. Interfaces* **2017**, *9*, 38706.